Article

Structure, Recognition Properties, and Flexibility of the DNA·RNA Hybrid

Agnes Noy, Alberto Prez, Manuel Mrquez, F. Javier Luque, and Modesto Orozco

J. Am. Chem. Soc., **2005**, 127 (13), 4910-4920• DOI: 10.1021/ja043293v • Publication Date (Web): 03 March 2005

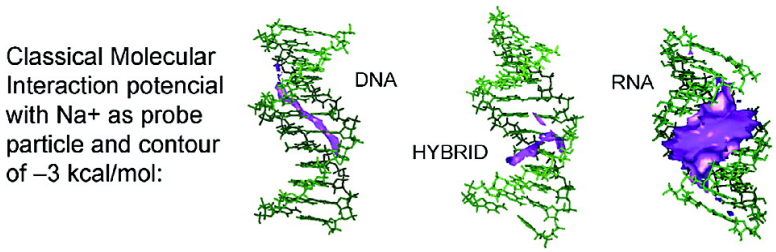

More About This Article

Additional resources and features associated with this article are available within the HTML version:

- Supporting Information
- Links to the 6 articles that cite this article, as of the time of this article download
- Access to high resolution figures
- Links to articles and content related to this article
- Copyright permission to reproduce figures and/or text from this article

View the Full Text HTML

J|A|C|S
ARTICLES
Published on Web 03/03/2005

Structure, Recognition Properties, and Flexibility of the DNA·RNA Hybrid

Agnes Noy,[†,‡] Alberto Pérez,[†,§] Manuel Márquez,[¶] F. Javier Luque,*[,§] and Modesto Orozco*[,†,‡]

Contribution from the Molecular Modeling and Bioinformatics Unit, Parc Cientific de Barcelona, Josep Samitier 1-5, Barcelona 08028, Spain, Departament de Bioquímica i Biología Molecular, Facultat de Química, Universitat de Barcelona, Martí i Franquès 1, Barcelona 08028, Spain, Departament de Farmàcia, Unitat de Fisicoquímica, Facultat de Farmacia, Universitat de Barcelona, Avgda Diagnonal 643, Barcelona 08028, Spain, and Los Alamos National Laboratory, Chemistry Division, Los Alamos, New Mexico 87545

Received November 8, 2004; E-mail: modesto@mmb.pcb.ub.es; javier@far1.far.ub.es

Abstract: Molecular dynamics is used to investigate the properties of the DNA·RNA hybrid in aqueous solution at room temperature. The structure of the hybrid is intermediate between A and B forms but, in general, closer to the canonical A-type helix. All the riboses exhibit North puckerings, while 2′-deoxyriboses exist in North, East, and South puckerings, the latter being the most populated one. The molecular recognition pattern of the DNA·RNA hybrid is a unique combination of those of normal DNA and RNA duplexes. Finally, the results obtained from essential dynamics and stiffness analysis demonstrate the large and very asymmetric flexibility of the hybrid and the strong predilection that each strand (DNA or RNA) has on the nature of their intrinsic motions in the corresponding homoduplexes. The implications of the unique structural and dynamic properties of the DNA·RNA hybrid on the mechanism of cleavage by RNase H are discussed.

Introduction

There are two major types of heterogeneous nucleic acids: hybrids and chimeras. In the former, not all the strands are of the same type (DNA or RNA), while in the latter, both DNA and RNA coexist in at least one of the strands. Hybrids and chimeras are minor species but play a key role in the cell life. Thus, transient DNA·RNA hybrids are formed as the RNA strand is created using the DNA template. Moreover, DNA replication relies on the existence of Okazaki's fragments, which are hybrid chimeras, where one strand is pure DNA and the other is an RNA−DNA chimera.[1] Furthermore, RNA viruses create DNA·RNA hybrids during retrotranscription, and the stability of these hybrid sequences is crucial in the replication cycle of these viruses.[2]

The large research effort spent in the past decade on the study of DNA·RNA hybrids is due not only to its biological relevance but also to its potential therapeutic application in antisense therapy. This new pharmacological strategy fights diseases by inactivation of the pathological messenger RNA (mRNA) following three main possible mechanisms:[3−8] (i) the degradation of the mRNA by means of the RISC-DICER mechanism, (ii) the sterical interference of translation or splicing by a complementary oligonucleotide (typically a DNA derivative) bound to the target mRNA, and (iii) the degradation of the mRNA bound to a complementary DNA analogue by RNase H, which is a specific enzyme that recognizes in a catalytically active manner only DNA·RNA hybrids and degrades the RNA strand of the hybrid. At the present time, most antisense treatments in clinical trials are based on the activation of the RNase H mechanism,[3−6] and then the design of stable and RNase H-susceptible hybrids is crucial.

The structure of DNA·RNA hybrids has been largely studied by means of experimental techniques. Early fiber diffraction data[9,10] suggested that the structure of the hybrid was very close to the A-form. This finding was also supported by many high-resolution X-ray data. Thus, the structure of an Okazaki's fragment, r(gcg)·d(TATACGC), solved by Rich's group[11] showed that it was very close to a canonical A-helix, with all sugars in the North conformation. The same conclusions were found by different crystallographers in other hybrid−chimeras.[12,13] Several pure DNA·RNA hybrids solved by X-ray

[†] Parc Cientific de Barcelona.
[‡] Facultat de Química, Universitat de Barcelona.
[§] Facultat de Farmacia, Universitat de Barcelona.
[¶] Los Alamos National Laboratory.

(1) Meselson, M.; Stahl, F. W. *Proc. Natl. Acad. Sci. U.S.A.* **1958**, *44*, 671.
(2) Alberts, B.; Bray, D.; Lewis, J.; Raff, M.; Roberts, K.; Watson, J. D. *Molecular Biology of the Cell*, 3rd ed.; Garland Publishing Inc.: New York, 1994.
(3) Biroccio, A.; Leonetti, C.; Zupi, G. *Oncogene* **2003**, *22*, 6579.
(4) Dean, N. M.; Bennett, C. F. *Oncogene* **2003**, *22*, 9087.
(5) Wagner, W. R.; Matteucci, M. D.; Grant, D.; Huang, T.; Froehler, B. C. *Nat. Biotechnol.* **1996**, *20*, 384.
(6) Taylor, M. F.; Wiederholt, K.; Sverdrup, F. *Drug Discovery Today* **1999**, *4*, 562.
(7) Yelin, R.; Dahary, D.; Sorek, R.; Levanon, E. Y.; Goldstein, O.; Shoshan, A.; Diber, A.; Biton, S.; Tamir, Y.; Khosravi, R.; Nemzer, S.; Pinner, E.; Walach, S.; Bernstein, J.; Savitsky, K.; Rotman, G. *Nat. Biotechnol* **2003**, *21*, 379.
(8) Carmichael, G. G. *Nat. Biotechnol.* **2003**, *21*, 371.
(9) Milman, G.; Langridge, R.; Chamberlin, M. J. *Proc. Natl. Acad. Sci. U.S.A.* **1967**, *57*, 1804.
(10) O'Brien, E. J.; MacEwan, A. W. *J. Mol. Biol.* **1970**, *48*, 243.
(11) Wang, A. H.; Fujii, S.; van Boom, J. H.; van der Marel, G. A.; van Boeckel, S. A.; Rich, A. *Nature* **1982**, *299*, 601.

10.1021/ja043293v CCC: $30.25

crystallography exhibit a typical A-form, with all riboses in the North conformation and all[14] or almost all[15−17] 2′-deoxyriboses with North puckerings. Surprisingly, data provided by low-resolution NMR, CD, and Raman[18−21] spectroscopies raise doubts on the X-ray structural picture of the hybrid; since all riboses are in the North conformation, a sizable portion of 2′-deoxyriboses exist in the South form, which is traditionally linked to the B-DNA. The same is found in recent NMR studies, which suggest a general structure of the hybrid intermediate between A and B canonical helices, with many characteristics of the A-form, but with important alterations in the grooves and with a large percentage of 2′-deoxyriboses in South conformations.[22−33]

The discrepancy between high-resolution NMR and X-ray studies cannot be fully explained from the differences in base sequence between hybrids solved by X-ray (typically with polypyrimidine in the DNA strand) and by NMR (generally more heterogeneous), as demonstrated by Gyi et al. and Fedoroff et al.[24,29,30] Clearly, experimental conditions are driving the structure toward the A and A/B conformations, suggesting a unique intrinsic structural plasticity in the DNA·RNA hybrid.

Though the discrepancy between NMR and X-ray results makes it difficult to define the major conformation of the hybrid in physiological conditions, it seems that NMR data provide an easier explanation of the fact that while DNA·RNA hybrids are degraded by RNase H, pure RNA duplexes are inhibitors.[34] Thus, according to NMR results, the smaller width of the minor groove in the hybrid compared to that in the pure RNA duplex has been considered to be the main structural feature to explain the different enzymatic susceptibility to RNase H.[16,21,22,24,33,34] However, recent studies have pointed out that factors other than the shape of the minor groove must also be involved,[32,33] thus raising doubts on the structural determinants that justify the degradation of the hybrid by RNase H.

Compared with the large amount of high-level experimental data, very few theoretical studies have examined the structure of the DNA·RNA hybrid. In a seminal paper, Cheatham and Kollman[35] reported 2 ns molecular dynamics (MD) trajectories of a 10-mer DNA·RNA duplex with Cornell's force field.[36] They found that, irrespective of the starting structure (pure A- or B-forms), the hybrid adopts a mixed A/B conformation, whose general conformation resembles that of the A-form, but with 2′-deoxyribose puckerings in the South region, thus supporting NMR data and previous JUNMA results by Lavery's group.[37] Identical conclusions were reached by Venkateswarlu et al. from 1 ns MD samplings[38] and more recently by Lane and co-workers[30] in a 2 ns MD study.

In this paper, we will present extended MD simulations of DNA·RNA hybrids starting from two different X-ray structures. Present trajectories (which expand to 10 times longer simulation time than previous ones) analyzed with the help of a powerful set of datamining algorithms allowed us to obtain a complete picture of the structure and dynamics of DNA·RNA hybrids. Our trajectories clearly converge to a conformation close to that suggested by NMR techniques. The structure, molecular recognition, and especially flexibility characteristics of the hybrid are determined and compared with those obtained for pure DNA and RNA duplexes built up with the equivalent base sequence. Finally, a tentative explanation of the specificity of RNase H for the DNA·RNA hybrid is provided.

Methods

Molecular Dynamics Simulations. Dodecamers of sequence r(cgcgaauucgcg)·d(CGCGAATTCGCG) were built using as template (i) the PDB crystal structure 1FIX[39] and (ii) an A-form conformation taken from Arnott's fiber diffraction data as implemented in the Biopolymer module of InsightII.[40] Choice of the Dickerson's sequence allowed us to compare the hybrid trajectories with those recently collected for the same sequence in DNA and RNA duplexes[41] and which will be used as reference for pure duplexes. Moreover, the selection of these two starting structures allows us to determine whether MD simulations[36,42] are consistent with crystal A-like structures or whether the trajectories spontaneously jump to the A/B NMR-like conformation.

The structures were first partially optimized (2000 cycles with restraints in the backbone) to avoid bad contacts emerging from changes in the sequence of the bases used in MD simulations with regard to that present in the X-ray crystallographic structure. The hybrids were surrounded by approximately 4400 water molecules and 22 Na^+ molecules placed in the regions of more electronegative potential (this generates rectangular boxes, $62 \times 62 \times 57$ (in angstroms)), with greater than 12 Å of waters from the DNA to the faces of the box. The hydrated systems were then optimized, heated, and equilibrated using our standard multistage protocol with length double than usual[43,44] to prevent any equilibration problem arising from the fact that we are studying hybrids and not homoduplexes. Then, two (11 and 5 ns) unrestrained MD simulations were run (the first nanosecond was considered extra equilibration in both cases). All MD simulations were performed in

(12) Egli, M.; Usman, N.; Zhang, S. G.; Rich, A. *Proc. Natl. Acad. Sci. U.S.A.* **1992**, *89*, 534.
(13) Egli, M.; Usman, N.; Rich, A. *Biochemistry* **1993**, *32*, 3221.
(14) Xiong, Y.; Sundaralingam, M. *Nucleic Acids Res.* **2000**, *28*, 2171.
(15) Conn, G. L.; Brown, T.; Leonard, G. A. *Nucleic Acids Res.* **1999**, *27*, 555.
(16) Horton, N. C.; Finzel, B. C. *J. Mol. Biol.* **1996**, *264*, 521.
(17) Katahira, M.; Lee, S. J.; Kobayashi, Y.; Sujeta, H.; Kyogoku, Y.; Iwai, S.; Ohtsuka, E.; Benevides, J. M.; Thomas, G. J. *J. Am. Chem. Soc.* **1990**, *112*, 4508.
(18) Chou, S. H.; Flynn, P.; Reid, B. *Biochemistry* **1989**, *28*, 2422.
(19) Chou, S. H.; Flynn, P.; Reid, B. *Biochemistry* **1989**, *28*, 2435.
(20) Hall, K. B.; McLaughlin, L. W. *Biochemistry* **1991**, *30*, 10606.
(21) Fedoroff, O. Y.; Salazar, M.; Reid, B. R. *J. Mol. Biol.* **1993**, *233*, 509.
(22) Fedoroff, O. Y.; Ge, Y.; Reid, B. R. *J. Mol. Biol.* **1997**, *269*, 225.
(23) Lane, A. N.; Ebel, S.; Brown, T. *Eur. J. Biochem.* **1993**, *215*, 297.
(24) Salazar, M.; Fedoroff, O. Y.; Miller, J. M.; Ribeiro, N. S.; Reid, B. R. *Biochemistry* **1993**, *32*, 4297.
(25) Gao, X.; Jeffs, P. W. *J. Biomol. NMR* **1994**, *4*, 367.
(26) Gonzalez, C.; Stec, W.; Kobylanska, A.; Hogrefe, R. I.; Reynolds, M.; James, T. L. *Biochemistry* **1994**, *33*, 1062.
(27) Gonzalez, C.; Stec, W.; Reynolds, M.; James, T. L. *Biochemistry* **1995**, *34*, 4969.
(28) Gyi, J. I.; Conn, G. L.; Lane, A. N.; Brown, T. *Biochemistry* **1996**, *35*, 12538.
(29) Gyi, J. I.; Lane, A. N.; Conn, G. L.; Brown, T. *Biochemistry* **1998**, *37*, 73.
(30) Gyi, J. I.; Gao, D.; Conn, G. L.; Trent, J. O.; Brown, T.; Lane, A. N. *Nucleic Acids Res.* **2003**, *31*, 2683.
(31) Cross, C. W.; Rice, J. S.; Gao, X. *Biochemistry* **1997**, *36*, 4096.
(32) Nishizaki, T.; Iwai, S.; Ohkubo, T.; Kojima, C.; Nakamura, H.; Kyogoku, Y.; Ohtsuka, E. *Biochemistry* **1996**, *35*, 4016.
(33) Szyperski, T.; Gotte, M.; Billeter, M.; Perola, E.; Cellai, L.; Heumann, H.; Wuthrich, K. *J. Biomol. NMR* **1999**, *13*, 343.
(34) Salazar, M.; Fedoroff, O. Y.; Zhu, L.; Reid, B. R. *J. Mol. Biol.* **1994**, *241*, 440.
(35) Cheatham, T. E.; Kollman, P. A. *J. Am. Chem. Soc.* **1997**, *119*, 4805.
(36) Cornell, W. D.; Cieplak, P.; Bayly, C. I.; Gould, I. R.; Merz, K. M.; Ferguson, D. M.; Spellmeyer, D. C.; Fox, T.; Caldwell, J. W.; Kollman, P. A. *J. Am. Chem. Soc.* **1995**, *117*, 5179.
(37) Sanghani, S. R.; Lavery, R. *Nucleic Acids Res.* **1994**, *22*, 1444.
(38) Venkateswarlu, D.; Lind, K. E.; Mohan, V.; Manoharan, M.; Fergurson, D. M. *Nucleic Acids Res.* **1999**, *27*, 2189.
(39) Horton, N. C.; Finzel, B. C. *J. Mol. Biol.* **1996**, *264*, 521.
(40) (a) Arnott, S.; Bond, P. J.; Selsung, E.; Smith, P. J. *Nucleic Acids Res.* **1976**, *3*, 2459. (b) *Insight II*; Accelrys Co.: San Diego, CA, 2004.
(41) Noy, A.; Perez, A.; Lankas, F.; Luque, F. J.; Orozco, M. *J. Mol. Biol.* **2004**, *343*, 627.
(42) Cheatham, T. E.; Cieplak, P.; Kollman, P. A. *J. Biomol. Struct. Dyn.* **1999**, *16*, 845.
(43) Shields, G. C.; Laughton, C. A.; Orozco, M. *J. Am. Chem. Soc.* **1997**, *119*, 7463.
(44) Shields, G. C.; Laughton, C. A.; Orozco, M. *J. Am. Chem. Soc.* **1998**, *120*, 5895.

the isothermic−isobaric ensemble (1 atm, 298 K). Periodic boundary conditions and the Particle Mesh Ewald (PME[45]) technique were used to treat long-range effects. All bonds were constrained using SHAKE,[46] which allowed us to use an integration time step of 2 fs. Parm99[36,42] and TIP3P[47] force fields were used to describe molecular interactions. Global translations were removed every 0.5 ns to remove erroneous partitions of the kinetic energy of the system. Since both trajectories converged to a similar region of the configurational space (see below), the structural and flexibility analyses were performed by using only the last 10 ns of the longest trajectory. Moreover, the base pairs at both 5′ and 3′ ends were not considered in the analysis. All trajectories were obtained using the SANDER module of the AMBER6.1 computer program.[48]

Structural and Energetic Analysis. Geometrical parameters sampled along the trajectories were studied using analysis modules in AMBER, the X3DNA program,[49] and *in house* software. Classical molecular interaction potentials were computed using the CMIP program[50] with Na^+ as a classical probe particle. Water densities around duplexes were determined by integrating the water population around polar atoms (cutoff distance of 3.5 Å) of the nucleic acids. Water residence times were computed by tracing all water molecules around polar groups following the standard procedure in the PTRAJ module of AMBER.

Essential Dynamics. Essential motions[41,51−53] were determined from principal component analysis (PCA) using covariance matrixes for common atoms of DNA and RNA (i.e., by excluding 5-methyl/H groups of T/U and 2′-OH/H groups in sugars). The diagonalization of the covariance matrix provided eigenvectors, which describe the nature of the essential movements, and eigenvalues, which determine the contribution of each essential movement to the positional variance of the trajectory. For two molecules of the same size, the number of eigenvectors necessary to explain a given positional variance indicates the complexity of the molecular motions; the larger the number of essential motions, the greater the complexity.

Eigenvectors of the same dimension obtained from two trajectories can be compared by means of the absolute and relative similarity indexes given in eqs 1 and 2,[51,54,55] which measure the similarity between the essential deformation pattern of the two systems.

$$\gamma_{AB} = \frac{1}{n}\sum_{j=1}^{n}\sum_{i=1}^{n}(\nu_i^A \cdot \nu_j^B)^2 \tag{1}$$

where ν_i^A is the unit eigenvector i of molecule A; n is the minimum number of essential motions that account for a given variance in the trajectory, and the dot denotes a scalar product.

$$\kappa_{AB} = 2\frac{\gamma_{AB}}{(\gamma_{AA}^T + \gamma_{BB}^T)} \tag{2}$$

where the self-similarity indexes, $\gamma_{AA}{}^T$, are calculated by comparing eigenvectors obtained with the first and second parts of the same trajectory.

Entropy Calculation. Intramolecular entropies were determined using Schlitter[56] and Andreocci−Karplus[57] methods (see eqs 3 and 4) and considering only atoms common to DNA and RNA (see above). The time dependence of the entropy estimates was corrected using the standard exponential extrapolation method.[51,58]

$$S \approx 0.5k\sum_i \ln\left(1 + \frac{e^2}{\alpha_i^2}\right) \tag{3}$$

$$S = k\sum_i \frac{\alpha_i}{e^{\alpha_i} - 1} - \ln(1 - e^{-\alpha_i}) \tag{4}$$

where $\alpha_i = \hbar\omega_i/kT$; ω denotes the eigenvalues obtained by diagonalization of the mass-weighted covariance matrix, and the sum extends to all nontrivial vibrations.

Stiffness Analysis. The positional fluctuations of atoms along the trajectory were used to derive force constants to describe the elastic deformability of the hybrid and their constituent strands.[51,59−63] The stiffness associated with the essential movements was determined from the eigenvalues obtained by diagonalization of the Cartesian covariance matrix[41] (see eq 5). Alternatively, the stiffness matrix K (with entries K_{ij}) associated with deformability along helical parameters was determined (see eq 6) by inverting the covariance matrix C (with entries $C_{ij} = \langle(X_i - X_{i_0})(X_j - X_{j_0})\rangle$). Diagonal elements in K represent contributions to deformation arising from individual helical variables, while off-diagonal components account for coupling terms. Note than once the force matrix is known, the deformation energy of a given configuration can be calculated by eq 7, where the subindex 0 stands for the equilibrium value.

$$K_{\lambda_i} = kT/\lambda_i \tag{5}$$

where λ_i is the eigenvalue (in angstroms^2) associated with the essential movement ν_i determined by diagonalization of the covariance matrix; T is the temperature (in kelvin); k is the Boltzmann constant, and $K_{\lambda i}$ is a force constant associated with the essential motion.

$$K = kTC^{-1} \tag{6}$$

$$E_{def} = \sum_i \frac{K_{ii}}{2}(X_i - X_{i_o})^2 + \sum_{i\neq j}\frac{K_{ij}}{2}(X_i - X_{i_o})(X_j - X_{j_o}) \tag{7}$$

Helical force constants were determined at the local (using local helical parameters as determined by X3DNA) and global (using the parameters defined by Lankas et al.[59,60]) levels. The local analysis was performed by using all of the snapshots collected from the MD trajectory.

Once the stiffness constants for global or local parameters are determined, the average deformation energy of the duplex can be

(45) Darden, T.; York, D.; Pedersen, L. *J. Chem. Phys.* **1993**, *98*, 10089.
(46) Ryckaert, J. P.; Ciccotti, G.; Berendsen, H. J. C. *J. Comput. Phys.* **1977**, *23*, 327.
(47) Jorgensen, W. L.; Chandrasekhar, J.; Madura, J. D.; Impey, R. W.; Klein, M. L. *J. Chem. Phys.* **1983**, *79*, 926.
(48) Case, D. A.; Pearlman, D. A.; Caldwell, J. W.; Cheatham, T. E., III; Ross, W. S.; Simmerling, C. L.; Darden, T. L.; Marz, K. M.; Stanton, R. V.; Cheng, A. L.; Vincent, J. J.; Crowley, M.; Tsui, V.; Radmer, R. J.; Duan, Y.; Pitera, J.; Massova, I.; Seibel, G. L.; Singh, U. C.; Weiner, P. K.; Kollman, P. A. *AMBER6*; University of California: San Francisco, CA, 1999
(49) Lu, X. J.; Shakked, Z.; Olson, W. K. *J. Mol. Biol.* **2000**, *300*, 819.
(50) Gelpi, J. L.; Kalko, S. G.; Barril, X.; Cirera, J.; de La Cruz, X.; Luque, F. J.; Orozco, M. *Proteins* **2000**, *45*, 428.
(51) Orozco, M.; Perez, A.; Noy, A.; Luque, F. J. *Chem. Soc. Rev.* **2003**, *32*, 350.
(52) Wlodek, S. T.; Clark, T. W.; Scott, L. R.; McCammon, J. A. *J. Am. Chem. Soc.* **1997**, *119*, 9513.
(53) Sherer, E. C.; Harris, S. A.; Soliva, R.; Orozco, M.; Laughton, C. A. *J. Am. Chem. Soc.* **1999**, *121*, 5981.
(54) Cubero, E.; Abrescia, N. G. A.; Subirana, J. A.; Luque, F. J.; Orozco, M. *J. Am. Chem. Soc.* **2003**, *125*, 14603.
(55) Rueda, M.; Kalko, S. G.; Luque, F. J.; Orozco, M. *J. Am. Chem. Soc.* **2003**, *125*, 8007.
(56) Schlitter, J. *Chem. Phys. Lett.* **1993**, *215*, 617.
(57) Andricioaei, I.; Karplus, M. *J. Chem. Phys.* **2001**, *115*, 6289.
(58) Harris, S. A.; Gavathiotis, E.; Searle, M. S.; Orozco, M.; Laughton, C. A. *J. Am. Chem. Soc.* **2001**, *123*, 12658.
(59) Lankas, F.; Sponer, J.; Hobza, P.; Langowski, J. *J. Mol. Biol.* **2000**, *299*, 695.
(60) Lankas, F.; Sponer, J.; Langowski, J.; Cheatham, T. E. *Biophys. J.* **2003**, *85*, 2872.
(61) Olson, W. K.; Gorin, A. A.; Lu, X. J.; Hock, L. M.; Zhurkin, V. B. *Proc. Natl. Acad. Sci. U.S.A.* **1998**, *95*, 11163.
(62) Matsumoto, A.; Olson, W. K. *Biophys. J.* **2000**, *83*, 22.
(63) For comparison purposes with present Figure 9, note that Figure 4 of ref 46 has a typo error, and values in the *y*-axis need to be multiplied by a factor of 10.

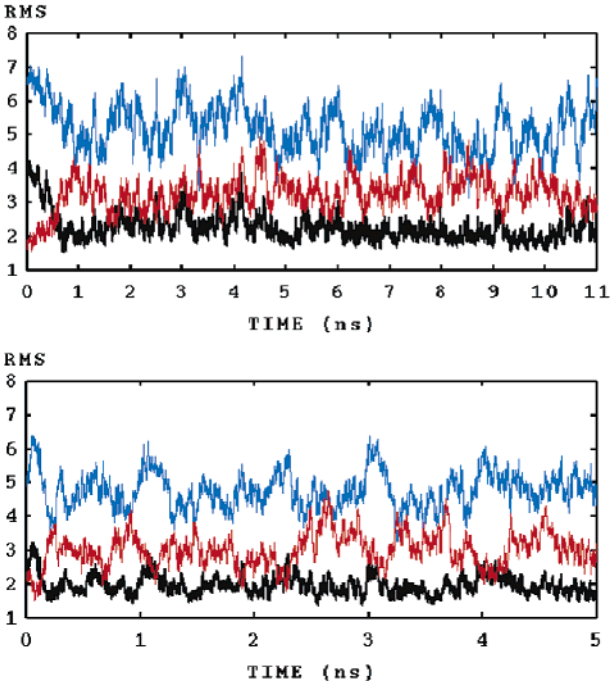

Figure 1. Root-mean-square deviations (RMSD for backbone atoms in angstroms) for the two hybrid trajectories; (top) starting 1FIX, and (bottom) from InsightII A-form, with respect to A (red), B (blue), and NMR (black; generated from 1EFS by (i) change of the sequence to the target one and (ii) restricted optimization of nucleobases to remove bad contacts) structures. Values displayed here correspond to the central 10-mer segment of the duplex.

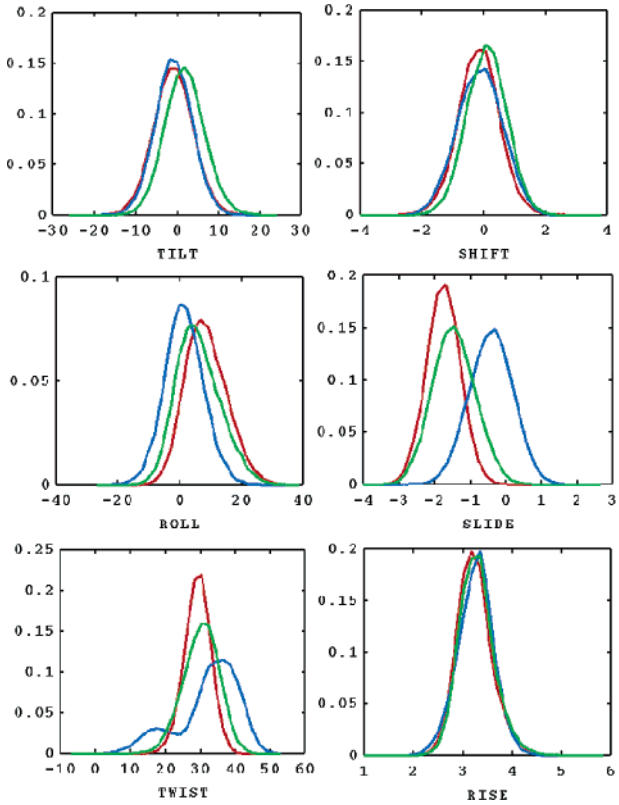

Figure 2. Distributions of selected local helical parameters in DNA_2, RNA_2, and DNA·RNA trajectories. Rotational values are in degrees, and the translational ones are in angstroms. DNA_2 (blue), RNA_2 (red), and hybrid (green).

computed considering a common limit of deformation for each helical coordinate. This limit should (i) make all helical deformation equally important in the definition of the distortion energy, and (ii) allow the comparison between DNA_2, RNA_2, and DNA·RNA stiffness. Thus, we defined the consensus perturbation for each helical parameter as twice the largest standard deviation found for this parameter in the three trajectories. Conformations are then randomly generated by moving randomly each individual helical parameter within these limits.

Results and Discussion

Convergence of the Trajectories. There is a clear displacement in the two trajectories (in less than 1 ns) from the A-form to an A/B conformation, closer to the A- than to the B-form, but clearly different from the canonical A-helix (see Figure 1). Both simulations sampled the same region of the configurational space, which is close to the conformation found in NMR experiments (1EFS[64] was used here for reference; see Figure 1). Analysis of the trajectories clearly demonstrated that, as previous MD simulations suggested,[30,36,41] the fast repuckering of the 2′-deoxyriboses from pure North to South/South-East conformations is responsible for the structural transitions detected in the simulations.

Taking data from our longest trajectory (very similar results can be obtained considering the 5 ns one starting from pure A-form), we can quantify deviations in the converged structure with respect to reference conformations. The average RMSD (values taken for the central 10-mer backbone (including C1′) in the last 10 ns of the trajectory) with respect to the starting conformation is 2.9 ± 0.5 Å, a value which is slightly larger than that found when RMSD is computed from a classical NMR (1EFS [64]) conformation (2.2 ± 0.3 Å). The RMSD with respect to the B-form is larger (5.1 ± 0.7 Å with respect to Arnott's values and 3.5 ± 0.6 Å with respect to the MD-averaged conformation of B-DNA) than that with respect to A-form (3.3 ± 0.4 Å from Arnott's[40] values and 2.8 ± 0.5 Å from the MD-averaged conformation of the A-RNA). In summary, MD simulations drive the structure of the hybrid from fiber or crystal conformations to NMR-like conformation, which is not a pure A-form, but that, in general, is clearly closer to this conformation than to the B-form.

General Structural Characteristics. Helical analysis shows that the average twist angle is ∼31°, which is close to that found for the RNA duplex (∼30°) and smaller than that for the DNA one (∼33°) (see Figure 2). With regard to slide, the hybrid is also closer to RNA than to DNA. For the rest of the local helical parameters, the hybrid is either intermediate between DNA and RNA or does not change significantly between the three kinds of duplexes (see Figure 2). The intermediate A/B character of the hybrid becomes more evident when looking to more general descriptors, such as the shortest C1′−C1′ intrastrand distance[41] or the global (see Methods) helical parameters (see Figure 3). Interestingly, compared with the DNA duplex, both RNA and hybrid duplexes seem to be less sequence-dependent, as reflected in a more normal distribution of some helical parameters, such as twist (see Figure 2).

There are several differences in the distribution of the backbone dihedral angles (available upon request) with respect to pure DNA and RNA duplexes. In general, the differences are due to a strong asymmetry between the two strands in the hybrid, which seems to retain some kind of predilection for the

(64) Hantz, E.; Larue, V.; Ladam, P.; Le Moyec, L.; Gouyette, C.; Huynh Dinh, T. *Int. J. Biol. Macromol.* **2001**, *28*, 273.

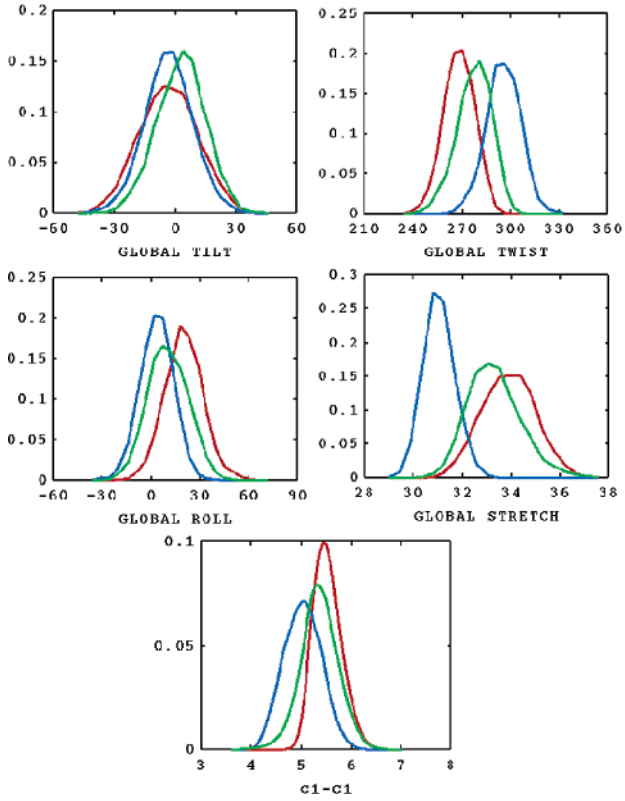

Figure 3. Distributions of selected global helical parameters in DNA_2, RNA_2, and DNA·RNA trajectories. Rotational values are in degrees, and the translational ones are in angstroms. See color code in Figure 2.

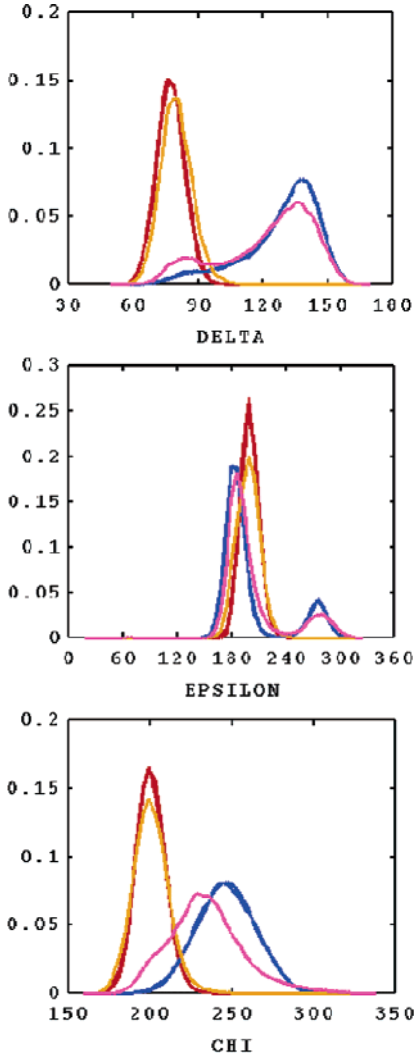

Figure 4. Distributions of selected backbone dihedrals in DNA_2, RNA_2, and DNA·RNA trajectories. Taking values for individual strands (the two DNA strand in DNA_2 (blue), the two RNA strands in RNA_2 (red), the DNA strand in the hybrid (magenta), and the RNA strand in the hybrid (orange). Values are in degrees.

distributions found in corresponding pure duplexes (see Figure 4 for selected examples). Such a predilection is clearly reflected in the sugar puckering since all riboses are found in the North conformation (as expected for RNA), while 2′-deoxyriboses mainly populate South and South-East conformations (only 8−9% is found in North conformations) (see Figure 5). The change between S ↔ E ↔ N puckerings of 2-deoxyriboses is very fast (subnanosecond time scale), which indicates that present results cannot be ascribed to limited sampling in our MD simulations (see Figure 5). We must also notice that the amount of East conformers in the DNA strand of the hybrid is not different than that detected in normal DNA duplexes, which supports suggestions by James and co-workers[26,27] that the anomalous sugar spectra found for the DNA·RNA hybrids are not due to a displacement of the 2′-deoxyriboses to the East conformation, but to a fast interchange between North and South puckerings.

The strand asymmetry in sugar puckering generates a unique groove distribution in the hybrid. The major groove is clearly wider than that of pure RNA and only ∼2 Å narrower than that of pure DNA (see Figure 6). The minor groove of the hybrid is ∼2 Å narrower than that of pure RNA and clearly wider than that of pure DNA. Very interestingly, the minor groove of the hybrid seems to be less sensitive to sequence effects (particularly to A-tracks) than does that of the DNA duplex (see Figure 6), leading to a more normal distribution in the hybrid. This difference is probably due to the geometrical restrictions imposed by the fixed conformation of the riboses in the RNA strand.

Molecular Recognition Properties. The unique groove geometry of the hybrid generates a special recognition pattern compared to DNA and RNA duplexes of the same sequence. This is noted in the cMIP distribution (Figure 7), which has characteristics of both DNA and RNA duplexes and an interesting asymmetry between strands in the major groove since the most favored region for interaction with small cations is not centered in the middle of the groove but displaced toward the RNA strand (see Figure 7). The hybrid is very well hydrated by an average number of 27.0 water molecules/nucleotide pair compared with values of 25.3 and 28.2 for DNA and RNA, respectively. In the minor groove, the amount of highly structured water is slightly larger (see Figure 7) for DNA than for RNA, the hybrid being in an intermediate situation. Due to the presence of the 2′-OH group, the backbone is better hydrated in RNA (12.8 waters/single strand) and in the RNA strand of the hybrid (12.4 waters) than in the DNA duplex (10.4 waters/single strand) or the DNA strand (10.6 waters) of the hybrid. The maximum water residence times around polar groups range from 100 ps to 1 ns, and no systematic differences are detected between DNA, RNA duplexes, and the hybrid.

Entropy Calculations. Schlitter and Andreocci-Karplus methods were used to estimate the intramolecular entropy of

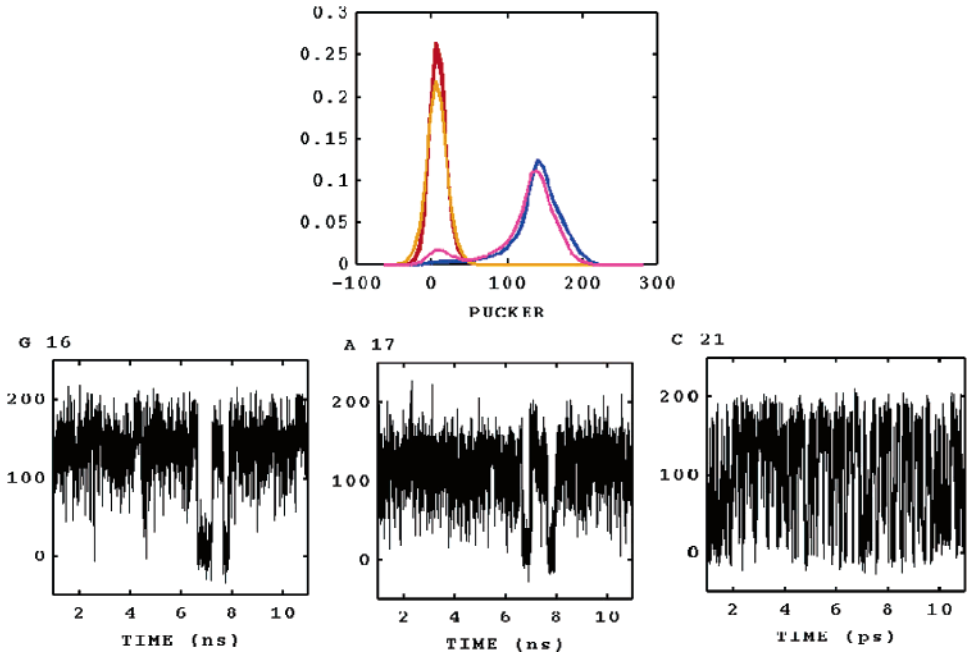

Figure 5. (Top panel) Distribution of phase angles (in degrees) in DNA_2, RNA_2, and DNA·RNA trajectories. Values are obtained by taking the two strands separately (see color codes in Figure 4). (Bottom panels) Evolution of the phase angle along the 11 ns hybrid trajectory for selected nucleotides.

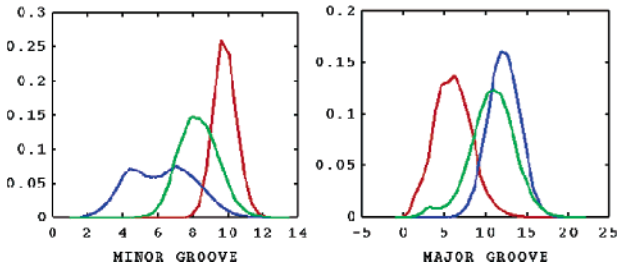

Figure 6. Distribution of minor and major groove widths in DNA_2, RNA_2, and DNA·RNA trajectories. Distances (in angstroms) are computed as the shortest P−P distance along the groove minus 5.8 Å (van der Waals radii of phosphates).

the duplexes. Both methods suggest that DNA is the most disordered structure, followed by the hybrid and finally by the RNA (Table 1). The difference in total entropy between RNA and DNA is 0.24 kcal/mol·K,[41] and 0.16 kcal/mol·K between RNA and the hybrid. Therefore, while structural parameters point out that the hybrid is closer to pure RNA, the hybrid is closer to pure DNA in terms of structural disorder. As found in a previous analysis of homoduplexes,[41] such an entropic difference arises from the backbone (entropy estimates obtained considering only the nucleobases are nearly identical for the three duplexes; see Table 1). Interestingly, when entropies are computed considering only the first three essential movements, DNA is the most ordered helix, while RNA and DNA·RNA show the same level of structural disorder. When the calculation includes the first 10 frequencies, the hybrid appears as the most disordered structure and RNA as the most ordered one. Clearly, entropy is not distributed uniformly in the three duplexes (see Figure 8), a fact that was already recognized in a previous study of DNA and RNA flexibility.[41]

The two strands of the hybrid retain the intrinsic flexibility in their respective homoduplexes. Thus, the DNA strand of the hybrid has an entropy 0.12 kcal/mol·K larger than that of the RNA strand (see Table 2). Quite impressively, the entropy estimates for the DNA and RNA strands of the hybrid nearly

Table 1. Intramolecular Entropies (in kcal/mol·K) Computed using Schlitter's (roman font) and Andreocci-Karplus's Methods (*italics*) for DNA, RNA, and HYBRID Double Strand and Extrapolated to Infinite Simulation Time (see Methods)[a]

	$S(t=\infty)$	$S(3)$	$S(10)$
DNA	2.14(0.05)	0.0328	0.0988
(all atoms)	*1.93(0.05)*	*0.0327*	*0.0983*
RNA	1.90(0.03)	0.0342	0.0976
(all atoms)	*1.71(0.03)*	*0.0340*	*0.0971*
HYBRID	2.06(0.03)	0.0341	0.0997
(all atoms)	*1.85(0.03)*	*0.0339*	*0.0993*
DNA	0.91(0.01)	0.0286	0.0849
(nucleobases)	*0.84(0.01)*	*0.0285*	*0.0845*
RNA	0.91(0.02)	0.0300	0.0860
(nucleobases)	*0.83(0.02)*	*0.0299*	*0.0856*
HYBRID	0.91(0.01)	0.0299	0.0858
(nucleobases)	*0.84(0.02)*	*0.0298*	*0.0853*
DNA	1.43(0.07)	0.0320	0.0962
(backbone)	*1.34(0.10)*	*0.0319*	*0.0958*
RNA	1.18(0.03)	0.0333	0.0944
(backbone)	*1.09(0.03)*	*0.0331*	*0.0940*
HYBRID	1.34(0.04)	0.0332	0.0973
(backbone)	*1.24(0.04)*	*0.0331*	*0.0968*

[a] Partial entropies were computed considering only nucleobases or backbone atoms. In all cases, values were determined considering all frequencies, as well as only the first 3 and 10 ones.

match the average values obtained for the same strands in homopolymers of the same sequence (see Table 2). Finally, the entropy contributions associated with the first 10 essential movements of the DNA and RNA strands of the hybrid follow very closely those observed for the same strands in homopolymers (see Figure 8). In summary, the two strands of the hybrid maintain their intrinsic entropy in pure duplexes, which is not much altered by the counterpart, and the global entropy properties of the hybrid should then be understood as a combination of the local entropies of the two strands.

Essential Dynamics. As previously found in other studies,[51,55] global twistings and bendings are the movements that explain most variances in the three duplexes. The first modes in all nucleic acids are associated with very small stiffness constants

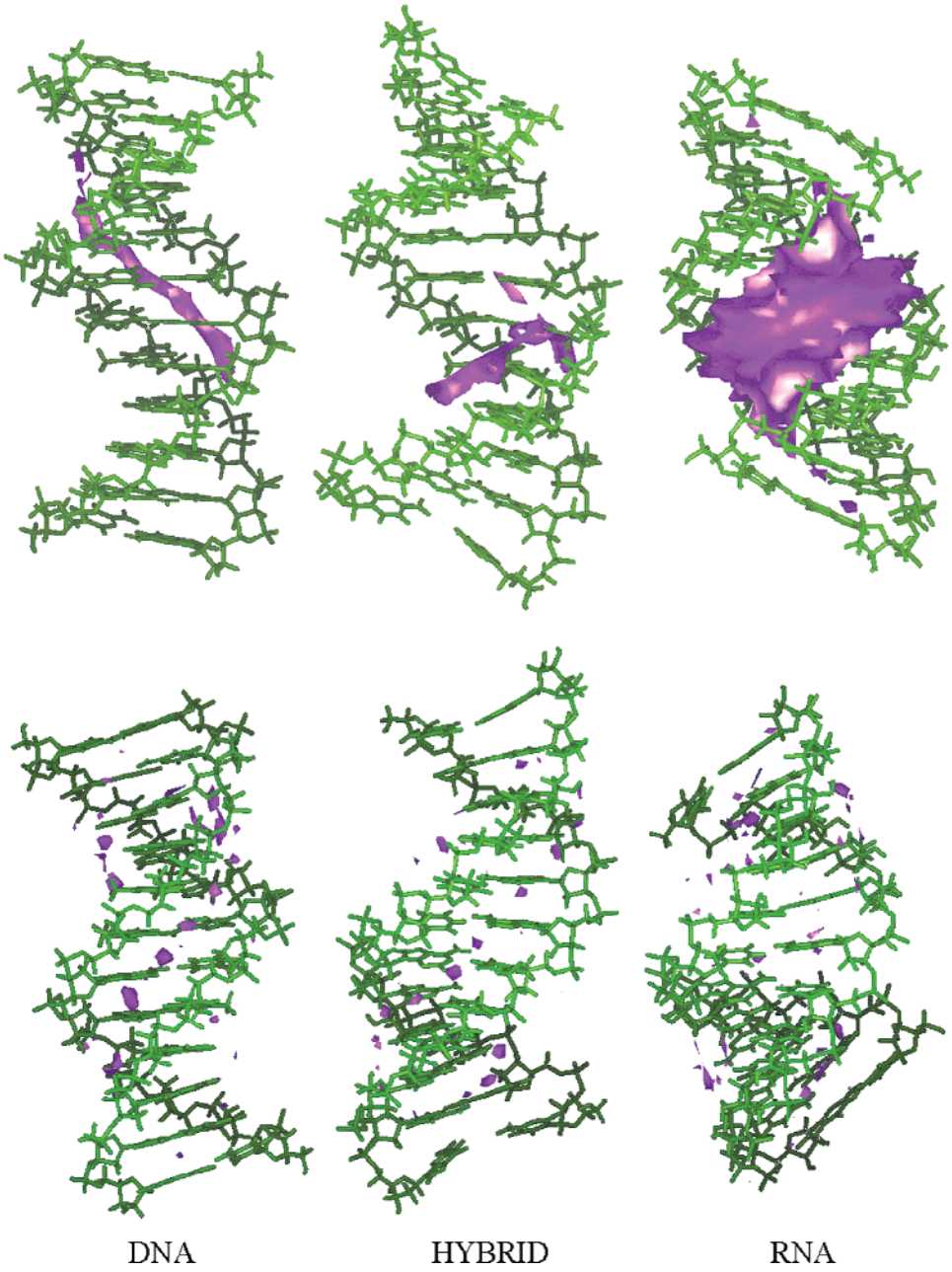

Figure 7. (Top) Classical Molecular Interaction Potential (in purple energy contour −3 kcal/mol), showing the best region for interaction of the different duplexes with a classical Na^+ probe. (Bottom) Solvation map (in purple density contour 2.5 g/cm^3) density for the three duplexes.

(below 10 cal/mol·Å^2; see Figure 9), reflecting the extreme plasticity of nucleic acids along their preferred deformation pathways.[63] As suggested by entropy plots (Figure 8), the DNA appears to be very stiff for the first deformation modes, but the situation changes for higher essential movements. The hybrid shows stiffness constants similar to those of the RNA for the first five components, while for lower modes, they approach those of the DNA homoduplex (see Figure 9).

Similarity measurements for the 10 first essential modes (those explaining more than 70% variance of all trajectories) reveal that the nature of these movements is quite common to the three duplexes, especially in movements involving nucleobases (see Table 3). The essential deformation modes of the hybrid are slightly more similar to those of the RNA than to those of the DNA (see Table 3). However, the hybrid is able to capture characteristics of the essential dynamics of DNA which were not present in the RNA duplex and vice versa. Thus, similarity indexes between the hybrid and the two homoduplexes are larger than that obtained between pure DNA and RNA duplexes, the difference being especially clear when a large number (500) of eigenvectors are used in the comparison (see Table 3).

The essential dynamics of the RNA and DNA strands of the hybrid is significantly different, creating a unique asymmetry in the essential deformation modes of the hybrid. Thus, the relative similarities, κ, between the DNA and RNA strands of the hybrid are ∼76% for 10 modes and 88% for 250 modes (see Table 3), while when the dynamics of the two complementary strands of pure DNA and RNA duplexes is compared, similarity indexes very close to 1.0 are obtained. The essential

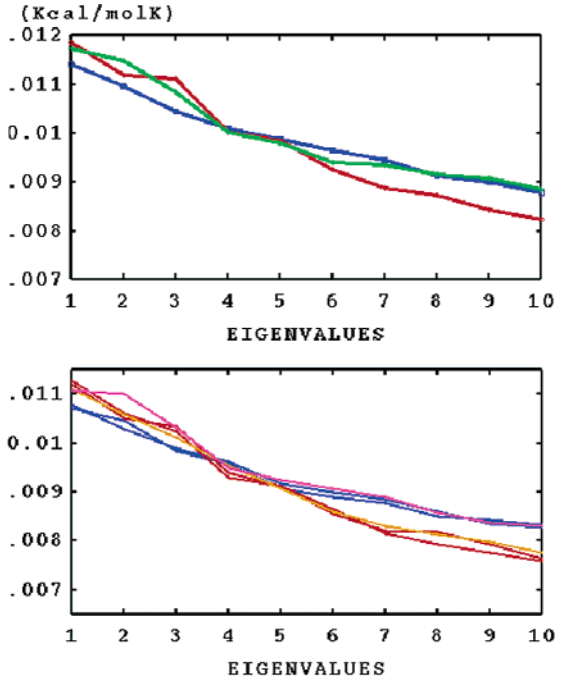

Figure 8. Entropies (in kcal/mol·K) assigned to different deformation modes of the three duplexes. (Top) Values for the two strands. (Bottom) Values for individual strands. Color code as in Figure 4.

Table 2. Same as Table 1, but Considering Each Strand Independently[a]

	$S(t=\infty)$	$S(3)$	$S(10)$
DNA	1.11(0.05)	0.0310	0.0928
(all atoms)	*1.03(0.07)*	*0.0308*	*0.0923*
RNA	0.99(0.02)	0.0321	0.0909
(all atoms)	*0.91(0.04)*	*0.0320*	*0.0905*
HYBRID DNA	1.12(0.02)	0.0324	0.0944
(all atoms)	*1.04(0.03)*	*0.0323*	*0.0940*
HYBRID RNA	1.00(0.02)	0.0318	0.0912
(all atoms)	*0.92(0.03)*	*0.0317*	*0.0908*
DNA	0.49(0.01)	0.0268	0.0786
(nucleobases)	*0.45(0.01)*	*0.0266*	*0.0782*
RNA	0.48(0.01)	0.0280	0.0793
(nucleobases)	*0.44(0.01)*	*0.0279*	*0.0789*
HYBRID DNA	0.49(0.01)	0.0281	0.0796
(nucleobases)	*0.45(0.01)*	*0.0280*	*0.0792*
HYBRID RNA	0.48(0.01)	0.0277	0.0787
(nucleobases)	*0.44(0.01)*	*0.0276*	*0.0783*
DNA	0.75(0.09)	0.0303	0.0906
(backbone)	*0.71(0.14)*	*0.0301*	*0.0901*
RNA	0.62(0.04)	0.0313	0.0877
(backbone)	*0.59(0.08)*	*0.0311*	*0.0873*
HYBRID DNA	0.75(0.03)	0.0317	0.0922
(backbone)	*0.70(0.04)*	*0.0316*	*0.0918*
HYBRID RNA	0.63(0.03)	0.0310	0.0882
(backbone)	*0.60(0.06)*	*0.0308*	*0.0877*

[a] For pure duplexes, values are the averages of the two strands.

movements of the RNA strand in the hybrid and in a pure RNA duplex are very similar (90% identity for 10 modes), while the maintenance of dynamics of the DNA strand is slightly worse (identity ~77% for 10 deformation modes (95% for 250 modes)). In summary, the two strands of the hybrid have a surprising tendency to maintain the essential dynamics of the DNA and RNA strands in pure homoduplexes. Such a predilection is especially strong for the RNA strand, whose deformability pattern in the hybrid is almost identical to that found in pure RNA duplexes.

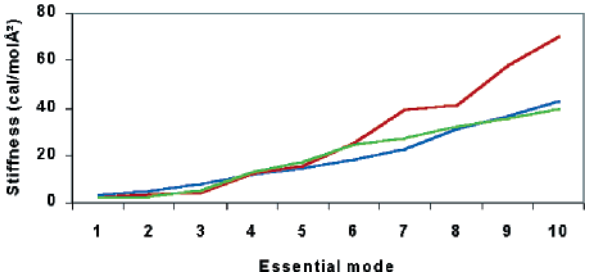

Figure 9. Force constants (in cal/mol·Å^2) assigned to the most essential movements of the three duplexes. Color code as in Figure 2.

Table 3. Relative (κ) Similarity Indexes between the Essential Movements of DNA, RNA, and HYBRID at the Duplex (top) and Single Strand (bottom) Levels[a]

	all atoms	nucleobases	backbone
	Duplex		
$\kappa_{HYBRID/RNA}$	0.788/*0.911*	0.859/*0.988*	0.805/*0.935*
$\kappa_{HYBRID/DNA}$	0.722/*0.921*	0.782/*0.990*	0.728/*0.919*
$\kappa_{DNA/RNA}$	0.682/*0.850*	0.701/*0.970*	0.692/*0.870*
	Single Strand		
$\kappa_{HYB\_RNA/RNA}$	0.904/*0.919*	0.875/*0.979*	0.866/ *0.961*
$\kappa_{HYB\_RNA/DNA}$	0.766/*0.852*	0.846/*0.984*	0.739/*0.851*
$\kappa_{HYB\_DNA/RNA}$	0.771/*0.866*	0.847/*0.986*	0.744/*0.883*
$\kappa_{HYB\_DNA/DNA}$	0.772/*0.952*	0.904/*0.982*	0.775/*0.961*
κ_{HYB_RNA/HYB_DNA}	0.763/*0.878*	0.842/*0.993*	0.769/*0.880*

[a] Values in roman correspond to the calculations using the first 10 modes, while values in italics are obtained considering the first 500 (duplex) or 250 (single strand) modes.

Table 4. Diagonal Elastic Force Constants for Deformations along a Reduced Set of Global Helical Parameters (angular force constants in cal/mol·deg^2 and displacement force constants in kcal/mol·Å^2) Computed for the Central 10-mer Portion of DNA, RNA, and HYBRID Duplexes[a,b]

	global tilt	global roll	global twist	global stretch
DNA	4.29(0.05)	5.92(0.07)	5.58(0.07)	1.51(0.039)
RNA	2.98(0.05)	5.74(0.11)	12.89(0.21)	0.80(0.009)
HYBRID	4.56(0.06)	4.76(0.12)	9.52(0.23)	0.79(0.018)

[a] Standard deviation values have been calculated by averages using different groups of snapshots taken every 5 ps. [b] The complete stiffness matrixes are available upon request.

Helical Stiffness. As noted in previous papers,[41,65] it is not clear whether DNA is more flexible than RNA in terms of global helical deformations. For the global twist, RNA is more rigid than DNA, but for global stretch and tilt, the reverse situation is found (see Table 4). Thus, DNA is more or less flexible than RNA depending on the type of global deformation. The hybrid has an intermediate behavior, though it is slightly closer to RNA than to DNA (see Table 4). Thus, the global twist of the hybrid is twice more difficult than for DNA and only 23% easier than for RNA. For the global stretch, the force constants in the hybrid and in RNA are identical and nearly one-half of that found for DNA. Finally, the hybrid is ~20% more flexible than both DNA and RNA in terms of global roll deformation and more rigid (50 and 20% relative to RNA and DNA, respectively) for changes in the global tilt (see Table 4). Considering a common isotropic distortion (i.e., a common distortion for all the duplexes defined to weight the same all the possible helical deformation;[41,63] see Figure 10), there are no clear differences between the global flexibility of DNA, RNA, and DNA·RNA duplexes (Figure 10).

(65) Perez, A.; Noy, A.; Lankas, F.; Luque, F. J.; Orozco, M. *Nucleic Acids Res.* **2004**, *32*, 6144.

Table 5. Diagonal Elastic Force Constants for Deformations along Local Helical Parameters of DNA, RNA, and HYBRID[a,b]

	tilt[c]	roll[c]	twist[c]	shift[d]	slide[d]	rise[d]
DNA	31.16(0.31)	18.50(0.15)	14.92(0.12)	1.22(0.01)	1.90(0.02)	7.20(0.01)
RNA	26.48(0.22)	15.06(0.08)	51.72(0.21)	1.37(0.01)	3.19(0.02)	6.18(0.06)
HYBRID	27.04(0.17)	12.82(0.12)	33.12(0.17)	1.58(0.01)	2.42(0.01)	7.01(0.05)

[a] Standard deviations are determined as noted in Table 4. [b] The complete stiffness matrixes are available upon request. [c] In cal/mol·deg^2 [d] In kcal/mol·Å^2

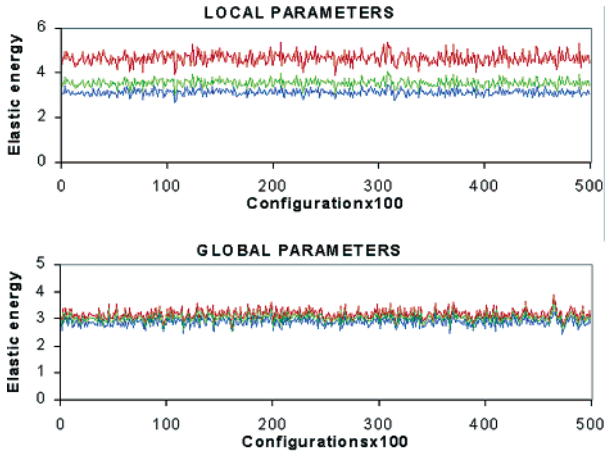

Figure 10. Elastic energy associated with helical isotropic distortions for the three nucleic acids. (Top) Perturbations in local helical parameters. (Bottom) Perturbations in global helical parameters. Perturbations along each helical variable are chosen as twice the largest standard deviation for this helical parameter in DNA_2, RNA_2, and DNA·RNA duplexes.

For most local helical parameters, RNA is stiffer than DNA, and in general, random local deformation is easier for DNA than for RNA[41,65] (see Table 5 and Figure 10). Once again, the behavior of the hybrid is intermediate between that of DNA and RNA (see Table 5), but the local pattern of deformability of the hybrid is unique, and not just a simple scaled average of that of DNA and RNA homoduplexes (Table 5). For example, deformation in rise and tilt is equally difficult for RNA_2 and the hybrid, but it is much easier to unwind or bend (twist and roll stiffness) the hybrid than a pure RNA duplex. The isotropic deformation energy of the hybrid is slightly closer to that of DNA than to that of the RNA duplex (see Figure 10), but this situation changes if the hybrid is deformed more along a helical coordinate than along the others (anisotropic perturbation). Once again,[41,65] the flexibility in nucleic acids emerges as a very complex concept especially for a molecule such as DNA·RNA with a very asymmetric pattern of deformability.

RNase H Susceptibility. RNase H has binding constants in the micromolar range for several oligonucleotides with A-like conformations, including RNA duplexes and DNA·RNA hybrids, but does not bind DNA duplexes[66−71] or other B-form nucleic acids.[70] The crystal structure of a RNase H suggests that the enzyme does not recognize a pure canonical A-form and that some distortion in the helix occurs.[72−75] It is also known that the enzyme does not show any marked sequence specificity[14,21,76,77] and is inactive against single-stranded oligonucleotides.[69,70] Finally, in DNA·RNA duplexes, only the RNA strand of the hybrid is degraded.[69,70]

All experimental data demonstrate that, despite the general similarity between RNA_2 and the hybrid, no appreciable amount of RNA duplex is degraded by the enzyme.[66−70,76] The reasons for this extreme specificity have been obscure for decades since it is not easy to find structural determinants which are different for DNA·RNA and RNA_2. Thus, all crystal structures of the DNA·RNA hybrid are nearly identical to those found for pure RNA duplexes (see Introduction). This fact could explain why both RNA duplexes and DNA·RNA hybrids are recognized by the enzyme, but does not justify why RNA duplexes are inhibitors and DNA·RNA hybrids are substrates.

Crystallization conditions might bias the conformation of the DNA·RNA hybrid, and both NMR and MD simulations suggest that the hybrid adopts in physiological conditions an intermediate A/B-form. In fact, analysis of NMR or MD structures allows the determination of a few structural differences between DNA·RNA and RNA_2, such as the narrower minor groove in the hybrid compared with RNA duplex. On the basis of this finding, several authors have suggested that a minor groove with a width of ∼8−9 Å is a necessary requisite for degradation by RNase H.[16,21−24] The cMIP profiles in Figure 7 confirm that the average recognition pattern of the minor groove of the hybrid is different than that of the RNA duplex, providing an apparent support to the hypothesis that a narrow minor groove is the structural determinant for RNase H specificity. However, a more detailed analysis of the structures shows that there is large overlap in the distribution of widths of DNA·RNA and RNA duplexes, and ∼20% of the time, the RNA duplex displays a minor groove with an "ideal" width of 8−9 Å (see Figure 6), which would imply some susceptibility of RNA duplexes to degradation by RNase H. Furthermore, cMIP calculations on hybrid−chimeras, which are recognized and degraded by RNase H,[32,33] show very anomalous minor grooves, leading to cMIP distributions far from that expected for a normal DNA·RNA hybrid (compare Figures 7 and 11) and, in some cases, identical to that of a normal RNA duplex (Figures 7 and 11). In summary, equilibrium geometry can easily explain why B-type helical structures do not bind the enzyme, but it cannot explain the discriminative ability of RNase H between RNA duplex and DNA·RNA hybrid.

Discarding sequence effects and the equilibrium geometry as the unique determinants for the specificity of RNase H, we can consider that the reduced stability of the DNA·RNA hybrid compared to that of the RNA homoduplex[78−81] can be a key

(66) Altmann, K. H.; Fabbrot, D.; Dean, N. M.; Geiger, T.; Monia, B. P.; Muller, M.; Nicklin, P. *Biochem. Soc. Trans.* **1996**, *24*, 630.
(67) Agrawal, S.; Iyer, R. P. *Pharmacol. Ther.* **1997**, *76*, 151.
(68) Crooke, S. T.; Bennett, C. F. *Annu. Rev. Pharmacol. Toxicol.* **1996**, *36*, 107.
(69) Han, G. W.; Kopka, M. L.; Cascio, D.; Grzeskowiak, K.; Dickerson, R. E. *J. Mol. Biol.* **1997**, *269*, 811.
(70) Lima, W. F.; Crooke, S. T. *Biochemistry* **1997**, *36*, 390.
(71) Stein, H.; Hausen, P. *Science* **1969**, *166*, 393.
(72) Ding, J.; Hughes, S. H.; Arnold, E. *Biopolymers* **1997**, *44*, 125.
(73) Ding, J.; Das, K.; Hsiou, Y.; Sarafianos, S. G.; Clark, A. D.; Jacobo-Molina, A.; Tantillo, C.; Hughes, S. H.; Arnold, E. *J. Mol. Biol.* **1998**, *284*, 1095.
(74) Jacobo-Molina, A.; Ding, J.; Nanni, R. G.; Clark, A. D.; Lu, X.; Tantillo, C.; Williams, R. L.; Kamer, G.; Ferris, A. L.; Clark, P. *Proc. Natl. Acad. Sci. U.S.A.* **1993**, *90*, 6320.
(75) Sarafianos, S. G.; Das, K.; Tantillo, C.; Clark, A. D.; Ding, J.; Whitcomb, J. M.; Boyer, P. L.; Hughes, S. H.; Arnold, E. *EMBO J.* **2001**, *20*, 1449.
(76) Oda, Y.; Iwai, S.; Ohtsuka, E.; Ishikawa, M.; Ikehara, M.; Nakamura, H. *Nucleic Acids Res.* **1993**, *21*, 4690.
(77) Roberts, W. R.; Crothers, D. M. *Science* **1992**, *258*, 1463.
(78) Riley, M.; Maling, B. *J. Mol. Biol.* **1966**, *20*, 359.

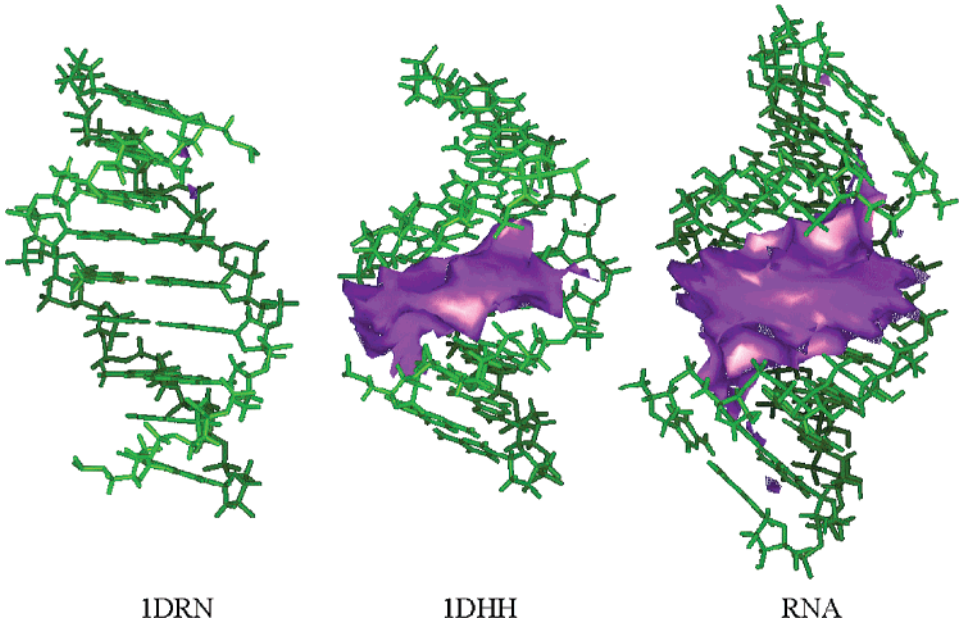

Figure 11. Classical Molecular Interaction Potential (energy contours −3 kcal/mol) for two hybrid structures known to be the substrate of RNase H (1DRN, 1DHH) and a reference RNA_2 duplex which is not degraded by the enzyme.

determinant of the different susceptibility of DNA·RNA and RNA_2 to the action of RNase H. This possibility is indirectly supported by the fact that modified oligonucleotides designed to make more stable DNA·RNA hybrids[5,67,68,82] fail to produce RNase H-susceptible hybrids. However, a few modified oligonucleotides have been generated displaying simultaneously good stability, specificity, and also RNase H susceptibility.[30,83−86] Thus, an intrinsic instability in the duplex does not appear to be a requisite for RNase H susceptibility.

In summary, to our understanding, and without rejecting a possible role for structure and for specific interactions (for example, those involving 2′-OH groups), flexibility emerges as the major differential trend that can use RNase H to discriminate between both duplexes.[32,33,87] Our MD simulations show that the pattern of deformability of the hybrid is quite different than that of a pure RNA duplex. Not only is the hybrid, in general, more flexible than the RNA duplex but also are there several specific local deformations which are much easier for the hybrid than for the RNA duplex, which provides more possibilities for deformability in the helix during the catalysis. Interestingly, our simulations strongly suggest that the RNA·DNA hybrid has a strong asymmetry in terms of flexibility between both strands. It is suggested that this unique asymmetry might be used by the enzyme to distinguish between the DNA and RNA strands, something that for a duplex showing a more symmetric pattern of flexibility will be very difficult.

(79) Sugimoto, N.; Nakano, S.; Katoh, M.; Matsumura, A.; Nakamuta, H.; Ohmichi, T.; Yoneyama, M.; Sasaki, M. *Biochemistry* **1995**, *34*, 11211.
(80) Nakano, S.; Kanzaki, T.; Sugimoto, N. *J. Am. Chem. Soc.* **2004**, *126*, 1088.
(81) Freier, S. M.; Altmann, K. H. *Nucleic Acids Res.* **1997**, *25*, 4429.
(82) McKay, R. A.; Miraglia, L. J.; Cummins, L. L.; Owens, S. R.; Sasmor, H.; Dean, N. M. *J. Biol. Chem.* **1999**, *274*, 1715.
(83) Moulds, C.; Lewis, J. G.; Froehler, B. C.; Grant, D.; Huang, T.; Milligan, J. F.; Matteucci, M. D.; Wagner, R. W. *Biochemistry* **1995**, *34*, 5044.
(84) Barnes, T. W.; Turner, D. H. *J. Am. Chem. Soc.* **2001**, *123*, 4107.
(85) Barnes, T. W.; Turner, D. H. *Biochemistry* **2001**, *40*, 12738.
(86) Tonelli, M.; Ulyanov, N. B.; Billeci, T. M.; Karwowski, B.; Guga, P.; Stec, W. J.; James, T. L. *Biophys. J.* **2003**, *85*, 2525.
(87) Nakamura, H.; Oda, Y.; Iwai, S.; Inoue, H.; Ohtsuka, E.; Kanaya, S.; Kimura, S.; Katsuda, C.; Katayanagi, K.; Morikawa, K.; Miyashiro, H.; Ikehara, M. *Proc. Natl. Acad. Sci. U.S.A.* **1991**, *88*, 11535.

Our results support a complex mechanism of action for RNase H. In a first step, the enzyme should bind any duplex showing a general conformation not far from the A-form and should reject B-type structures. In a second step, the enzyme should distort the duplex in a very asymmetric way, leaving the rigid RNA near the cleavage site while the DNA strand is pointed to the exterior. It is expected that this type of deformation will be too energetically costly for the rigid RNA duplex. Overall, we suggest the differential flexibility of RNA duplex and the hybrid, and especially, the asymmetry in the flexibility pattern of the latter constitutes the basis for the selective mechanism of action of RNase H. We propose that future designs of oligonucleotides for antisense purposes should explicitly consider these flexibility issues to guarantee the enzymatic susceptibility of the resulting hybrid.

Conclusions

Extended state-of-the-art MD simulations are able to reproduce with accuracy the structural properties of DNA·RNA hybrids, even when the starting conformation is far from the equilibrium conformation in solution.

The equilibrium geometry of the hybrid is closer to the A-form than to the B-form. All riboses show North puckerings, but 2′-deoxyriboses are mostly in the South and South-East regions, which lead to the definition of grooves intermediate to those typical of the A- and B-forms.

The flexibility of the DNA·RNA hybrid is unique and not a simple average of that of pure DNA and RNA hybrids. Quite surprisingly, each strand in the hybrid maintains well its essential dynamics in pure duplexes, which generates a strong asymmetry in the pattern of deformability of the helix.

Analysis of the different putative mechanisms that will allow RNase H to distinguish between different duplexes strongly suggests that while equilibrium structure can be enough for the enzyme to discard DNA_2, only the differential flexibility pattern can justify the ability of RNase H to discriminate between DNA·RNA and RNA_2.

Acknowledgment. We thank Dr. Chattopadhyaya for helpful discussions, and the Centre de Supercomputació de Catalunya for computer resources. We also thank the financial support of the Spanish Ministry of Education and Science (SAF2002-04282; BIO2003-06848), Fundació La Caixa, and Fundación BBVA. A.N. is a fellow of the Spanish Ministry of Education and Science, and A.P. is a DURSI fellow.

JA043293V